Stochastic homogenization of polymeric composites with randomly ellipsoidal reinforcement

***Damian Sokołowski[1] and †Marcin Kamiński[1]**

[1]Department of Structural Mechanics, Łódź University of Technology
Faculty of Civil Engineering, Architecture and Environmental Engineering
Al. Politechniki 6, 90-924 Łódź, Poland
*Presenting author: sokolowski.dmn@gmail.com
†Corresponding author: marcin.kaminski@p.lodz.pl

Abstract

The principle aim of this paper is determination of the basic probabilistic characteristics of homogenized stiffness tensor in particulate composites with ellipsoidal reinforcement and uncertain aspect ratio. A second objective is determination of susceptibility of this stiffness tensor to changes in this aspect ratio and type of reinforcing ellipsoid with spheroidal geometry, which include prolate and oblate; this is done for a wide range of ratio of main axes from 50:1 till 1:7. The homogenization problem is solved via the FEM with use of a cubic unitary single-particle Representative Volume Element (RVE) of the polymer and its 3D homogenization scheme is based on numerical determination of strain energy in the RVE under uniaxial and biaxial unitary stretch. Type and number of Finite Elements is optimized via the relative FEM error study so that its impact on probabilistic calculus is minimized and two different Finite Element types are used, i.e. 20-noded brick and 10-noded tetrahedral elements; strain energies are further used for determination of a homogenized orthotropic stiffness tensor. Probabilistic calculus is made with three independent approaches, the Iterative Stochastic Finite Element Method (ISFEM), the crude Monte-Carlo simulation and the semi-analytical method. A set of FEM solutions is available in probabilistic context upon application of the Response Function Method (RFM), where optimized polynomial approximations of the homogenized tensor components are recovered in the system MAPLE thanks to the Least Squares Method (LSM). RFM polynomial order is optimized via simultaneous maximization of correlation and minimization of LSM error and variance. A random aspect ratio is considered Gaussian, with mean value of 2 and coefficient of variation of aspect ratio smaller or equal to 0.15. We investigate numerically (1) if the resulting homogenized characteristics are also Gaussian, (2) how a change in aspect ratio affects the stiffness tensor in context of the probabilistic analysis and (3) if the homogenization increases the input uncertainty. We determine expected values, coefficients of variation, skewness and kurtosis for all available components of the effective elasticity tensor in 3D homogenization problems – all as functions of the coefficient of random dispersion for the input random parameter (aspect ratio of reinforcement).

Keywords: **Stochastic Finite Element Method, probabilistic homogenization, particulate composites, ellipsoidal reinforcement.**

Introduction

Homogenization technique serves for determination of the effective properties of all materials whose internal composition is characterized by some repeatable pattern. It is predominantly used in composites or advanced textiles. Properties considered by this method include mechanical [1], electrical [2], thermal [3] or coupled characteristics determined for linear or

non-linear [4][5] regime of such materials. Most of studies concern purely deterministic homogenization, but some of them also include randomness in their geometry, composition, reinforcement [6] or interphases [7]. They differ from the others at least by inclusion of a statistical scattering in the output that defines the bounds of properties for the considered materials together with some probability information. Then, they may possibly serve for determination of the material safety factors or the Probability Density Function of its properties and provide necessary safety margins into the design process. Some studies are also focused purely on determination of the Representative Volume Element (RVE) size [8] or discuss its effective generation techniques [9] so that the level of computational accuracy may be weighted by the available computational power. Homogenization of contemporary materials is only occasionally analytical as in [10]. This is because the RVEs are usually composed of several random phases with complex shapes or with multiple, randomly distributed inclusions or pores for which analytical calculus is simply unavailable. Instead, the RVE is modelled numerically, preferably with the Finite Element Method (FEM), and computed for the predefined load steps with specific boundary conditions. Only then these results are analytically converted and effective properties calculated. The FEM is leading for this application because of the ease of modelling and availability of commercial and non-commercial systems. Particulate composites are commonly homogenized on the basis of multi-particle RVEs [11] with particles of spherical as well as ellipsoidal shapes and different aspect ratios or orientation [12]. Such an approach ensures a more realistic representation of the composite then for the single-particle RVE but also includes an input randomness. This is because there is no certainty that, even most carefully chosen RVE, will exactly define the internal structure of each specimen. This is usually disregarded in current studies, where only one or at most several internal compositions are considered in the final computations and such an approach reduces their applicability to the mean characteristics with no information of dispersion at all. Lack of such works is evident and this is why randomness is introduced in this study in the form of an uncertain aspect ratio of the reinforcing particle. Additionally, properties of the matrix are also parametric with three mean values of its Young modulus and Poisson ratio. This is done on the basis of single particle RVE because of the computational intensity required for retrieval of the random characteristics, where each realization must be repeated multiple times with a variable input random parameter in the fashion very similar to the parametric design. These computations serve to check the probabilistic response of the homogenized (effective) stiffness tensor for the composite with the High Density Polyurethane (HDPU) matrix that is periodically reinforced with Carbon Black (CB) particles of ellipsoidal shape. Probabilistic calculations are made with three concurrent methods, which enables validation of each for the first four probabilistic moments and coefficients of the effective elasticity tensor.

Problem formulation and modeling details

Let us consider a periodic material composed of two phases, the matrix Ω_m and the reinforcement Ω_p in the form of ellipsoidal particles that remain both in their linear regime. Such a composite is approximated with a single particle Representative Volume Element (RVE) that permits retrieval of its mechanical properties, namely the effective stiffness tensor C_{ij}^{eff}. Once such a particle is placed centrally in this RVE, this stiffness tensor is orthotropic with 9 independent components, which are further reduced to 6 when two minor axes of the reinforcing particle have the same length (constitute a spheroid). They can be represented in the Voigt notation as C_{11}^{eff}, C_{22}^{eff}, C_{12}^{eff}, C_{13}^{eff}, C_{23}^{eff}, C_{44}^{eff} and C_{55}^{eff}, where the first pair of coefficients correspond to the uniaxial tensional stretches, second pair – to uniaxial shearing stretches and the last pair – to the biaxial tensional stretches. All the other components of the

effective stiffness tensor of such a material are null. Magnitude of this stiffness tensor for a strictly defined volume fractions of phases is lead by the aspect ratio A_r and orientation of the reinforcing particles. This study focuses on the first of these – the aspect ratio, which is considered here uncertain according to the Gaussian Probability Density Function (PDF)

$$p_b(x) = \frac{1}{\sigma(A_r)\sqrt{2\pi}} \exp\left(-\frac{(x - E[A_r])^2}{2\sigma^2(A_r)} \right); \; x \in \Re. \tag{1}$$

This is done because the dispersion of geometry of reinforcement is considerable in the contemporary composites. Its basic probabilistic moments and coefficients could be computed successively from the below formulas. First, the expected value of this aspect ratio could be retrieved as [13]

$$\mathrm{E}[A_r] = \int_{-\infty}^{+\infty} A_r \; \mathrm{p}_w(\mathrm{x}) \mathrm{dx} = \mu(A_r) \equiv \frac{1}{M} \sum_{i=1}^{M} A_r^{(i)}. \tag{2}$$

It could be then used to compute variation of A_r

$$\mathrm{Var}(A_r) = \int_{-\infty}^{+\infty} \left(A_r - \mathrm{E}[A_r] \right)^2 \mathrm{p}_w(\mathrm{x}) \mathrm{dx} \equiv \frac{1}{M-1} \sum_{i=1}^{M} \left(A_r^{(i)} - E[A_r] \right)^2, \tag{3}$$

and then converted to the coefficient of variation in a following way

$$\alpha(A_r) = \frac{\sqrt{\mathrm{Var}(A_r)}}{\mathrm{E}[A_r]} \tag{4}$$

With their use, the higher order coefficients of skewness β and kurtosis κ could be computed

$$\beta(A_r) = \frac{\mu_3(A_r)}{\sigma^3(A_r)} = \frac{\mathrm{E}[A_r^3] - 3\mu(A_r)\sigma^2(A_r) - \mu^3(A_r)}{\sigma^3(A_r)}; \; \kappa(A_r) = \frac{\mu_4(A_r)}{\sigma^4(A_r)} - 3, \tag{5}$$

Uncertainty of the aspect ratio A_r invokes uncertainty in the homogenized stiffness tensor, which is no more deterministic. Instead it could be defined by the first four probabilistic moments and coefficients, i.e. $E(C_{ij}^{eff})$, $\alpha(C_{ij}^{eff})$, $\beta(C_{ij}^{eff})$ and $\kappa(C_{ij}^{eff})$, where the expected value $E(C_{ij}^{eff})$ serves as the indicator of the most probable magnitude of C_{ij}^{eff}. They are all recovered in this study by triple computations consisting of the Iterative Stochastic Finite Element Method (ISFEM) with use of the statistically optimized 6th order [14], the crude Monte-Carlo simulation with 350 000 trials and the semi-analytical method with a direct differentiation of the characteristics from the response polynomial. An entire probabilistic calculus is based on the same response functions for each stiffness tensor coefficient, but calculations of the alternative methods are kept independent. This enables verification of the results of each of them and definition of a practical range of probabilistic moments. Discontinuous form of $E(A_r)$ and $Var(A_r)$ proposed on the right of eqn (1) and eqn (2) proves useful for the MCS, while the continuous one – in the ISFEM and the AM.

Mechanical properties of this linear composite include Young modulus and Poisson ratio. Reinforcing particle is defined by one set of parameters, $E_p = 10\ GPa$ and $\upsilon_p = 0.3$, while the matrix by three sets $[E_m, \upsilon_m] \in \{[4.4\ MPa,\ 0.374], [4.0\ MPa, 0.34], [3.6\ MPa, 0.306]\}$. Volume fraction of the matrix is set to 0.99 and of the particle - as 0.01 of the entire composite. Mesh of this composite (see Figure 1) is made of over 40 000 20-noded brick finite elements C3D20 with a second-order (full) stress approximation for all the 13 RVEs with modified aspect ratio of reinforcing particle. It was optimized via a FEM error study with 1st and 2nd order tetrahedral as well as hexahedral mesh of the RVE. This was done for three aspect ratios, the expected value of $A_r = \mathbf{\frac{2}{1}}$, for the highly prolate particle with $A_r = \mathbf{\frac{7}{1}}$ and also for the highly oblate particle with $A_r = \mathbf{\frac{1}{50}}$ to ensure applicability of this mesh for an entire range of aspect ratios considered here. Figure 1 shows the three sections of RVEs for these three aspect ratios indicating the applied mesh and shapes of particles. Horizontal axis

x_2 on this graph corresponds to C_{22}^{eff} and the vertical one x_1 – to C_{11}^{eff}. Reinforcing particle is placed centrally to ensure an orthotropic form of the homogenized stiffness tensor C_{ij}^{eff}.

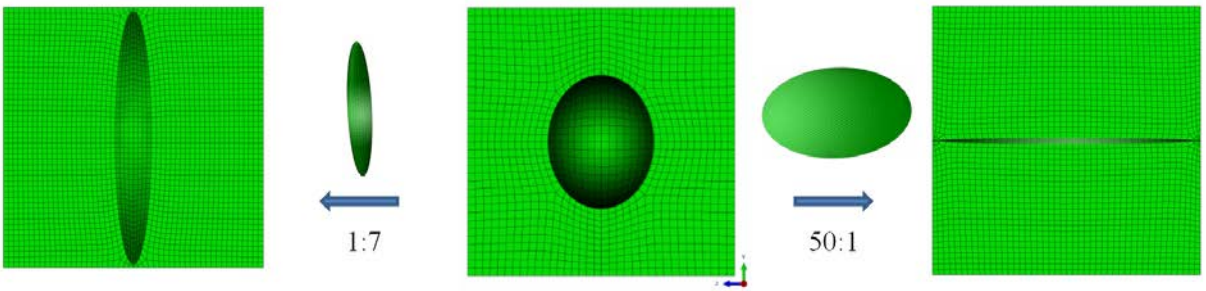

Figure 1. Discretization and range of reinforcing particle aspect ratio A_s.

Computational experiments are arranged in the following way. Firstly the FEM results are obtained for a set of 13 reinforcing particle aspect ratios $A_s \in \left\{\frac{1}{7}, \frac{1}{6.5}, \frac{1}{6}, \frac{1}{4}, \frac{1}{2}, \frac{1}{1}, \frac{2}{1}, \frac{5}{1}, \frac{15}{1}, \frac{25}{1}, \frac{35}{1}, \frac{45}{1}, \frac{50}{1}\right\}$ and the same volume fraction of the reinforcing particle for the relevant unitary stretches. Secondly, strain elastic energies are retrieved from the RVE and they are used in homogenization to retrieve the effective orthotropic stiffness tensor C_{ij}^{eff} composed of 6 independent coefficients. A set of discrete results of C_{ij}^{eff} is then approximated with use of Response Function Method (RFM), where optimized polynomial approximations of the homogenized tensor components are recovered with the Weighted Least Squares Method (WLSM). At the end, triple probabilistic computations are performed in the symbolic computer algebra program MAPLE 2017® returning the first four probabilistic moments and coefficients of the homogenized stiffness tensor C_{ij}^{eff}. This procedure is repeated for three sets of mechanical properties of the matrix and probabilistic characteristics are plotted on the graphs with relation to the uncertain aspect ratio of the particle. Weighting type of WLSM is similar to Dirac function with weights $\boldsymbol{w} \in \{\mathbf{1}, \mathbf{1}, \mathbf{1}, \mathbf{1}, \mathbf{1}, \mathbf{1}, \mathbf{12}, \mathbf{1}, \mathbf{1}, \mathbf{1}, \mathbf{1}, \mathbf{1}, \mathbf{1}\}$ so that the expected value placed in the middle has the same weight as the remaining results. Volume fraction of the reinforcement is kept exactly the same for all the aspect ratios to exclude its influence on the results. A separate polynomial is chosen for all of the 18 sets of results composed of three groups, each with two stiffness coefficients C_{ij}^{eff} (6 in total). These groups are formed because their stiffness tensor coefficients correspond to stretches coming from the same morphology, i.e. 1. uniaxial tensional stretches $\left(C_{11}^{eff} \text{ and } C_{22}^{eff}\right)$, 2. biaxial tensional stretches $\left(C_{12}^{eff} \text{ and } C_{13}^{eff}\right)$ and 3. uniaxial shearing stretches $\left(C_{44}^{eff} \text{ and } C_{55}^{eff}\right)$. A sample response functions for C_{12}^{eff} and C_{13}^{eff} with Young modulus of the matrix $E_m = 4.0\ MPa$ and $\upsilon_m = 0.34$ is given below

$$F_{C_{12}^{eff}}^{WLSM} = 3.213713088792 \cdot 10^6 - 1638.14409991523 \cdot A_r + 169.16048601791 \cdot {A_r}^2 - 7.18211669828524 \cdot {A_r}^3 + 0.133618128634940 \cdot {A_r}^4 - 0.000907865453443940 \cdot {A_r}^5. \quad (6)$$

$$F_{C_{13}^{eff}}^{WLSM} = 3.20891922978851 \cdot 10^6 + 2970.83491907751 \cdot A_r + 38.3393705910314 \cdot {A_r}^2 - 3.25681924655126 \cdot {A_r}^3 + 0.0437294660806783 \cdot {A_r}^4 - 0.000899175594518506 \cdot {A_r}^5. \quad (7)$$

An order of the approximating polynomial is optimized with simultaneous maximization of correlation and minimization of WLSM variance and error, where the precedence order is following: first correlation, second WLSM variance and third WLSM error. Polynomial approximations utilized for optimization ranged from full 1st order till full 12th order ones and

the unquestionably best fitting is ensured the 5th order polynomial. In most cases it ensured an exceptionally high correlation of at least 0.99, which proves smaller only for C_{12}^{eff} and C_{44}^{eff} but never lower than 0.89. There exists only one special case, i.e. C_{11}^{eff}, where the 7th order full polynomial is a little better than the 5th – correlation is higher on the 5th decimal number and its total error of WLSM is also smaller by 36%.

Results

A numerical example is targeted principally for a High Density Polyurethane (HDPU) reinforced with the Carbon Black and is chosen because of its relevance and applicability especially in the tire industry. Final results of the effective stiffness tensor C_{ij}^{eff} are summarized on the below graphs and include its first four probabilistic moments and coefficients, which are the expected value $E(C_{ij}^{eff})$, coefficient of variation $\alpha(C_{ij}^{eff})$, skewness $\beta(C_{ij}^{eff})$ and kurtosis $\kappa(C_{ij}^{eff})$. They are all shown as a function of the input coefficient of variation of particle aspect ratio $\alpha(A_r)$ for three different sets of mechanical properties of the linear matrix, i.e. for Young modulus of the matrix $E_m \in \{3.6, 4.0, 4.4\}$ MPa and Poisson ratio of $\nu_m \in \{0.374, 0.34, 0.306\}$, whose middle value represents properties of the High Density Polyurethane (HDPU). They are presented separately for 6 relevant stiffness tensor components placed in pairs on adjacent Figures (see for example Figure 2 and Figure 3). The graphs are ordered for an increasing probabilistic order and each characteristic is presented for three probabilistic methods. The first is the Iterative Stochastic Finite Element Method (ISFEM) with a caption of SPT, the second - Monte-Carlo simulation captioned by MCS and the third - semi-analytical approach with a caption of AM. These methodologies are differentiated by symbols on the below graphs and the sets of mechanical properties of the matrix are distinguished by colors.

The expected values $E(C_{ij}^{eff})$ are depicted on Figure 2 till Figure 7. They are generally unaffected by the increase of the input uncertainty with only a slight decrease below 1%. All three probabilistic methods return here perfectly coinciding results irrespectively to the input uncertainty and mechanical properties of the matrix. Obviously, together with an increase of these mechanical characteristics increase also all the expected values $E(C_{ij}^{eff})$. The rate of increase is much higher for the expectation (total increase of 155% – 212%) than for the stiffness tensor coefficients (total increase of 122%). This is, however, weighted by the volume fraction of the matrix in the entire composite equal to 0.99. Quite unexpectedly, the differences in relation of the homogenized stiffness tensor with the aspect ratio for the same groups of coefficients result only in marginal changes of the corresponding expectations (see for example Figure 6 and Figure 7). The highest expectations of over 8.1 kPa is reported for uniaxial tension coefficients C_{11}^{eff} and C_{22}^{eff}. The ones corresponding to biaxial stretches $(C_{12}^{eff}$ and $C_{13}^{eff})$ are almost twice smaller and the shearing ones – 3.5 times smaller.

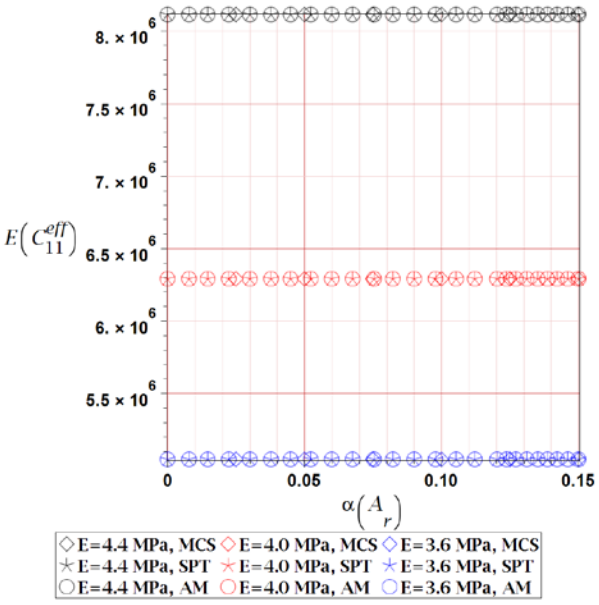

Figure 2. Expected value $E\left(C_{11}^{eff}\right)$ for an increasing matrix Young modulus E_m w.r.t. coefficient of variation of particle aspect ratio $\alpha(A_r)$.

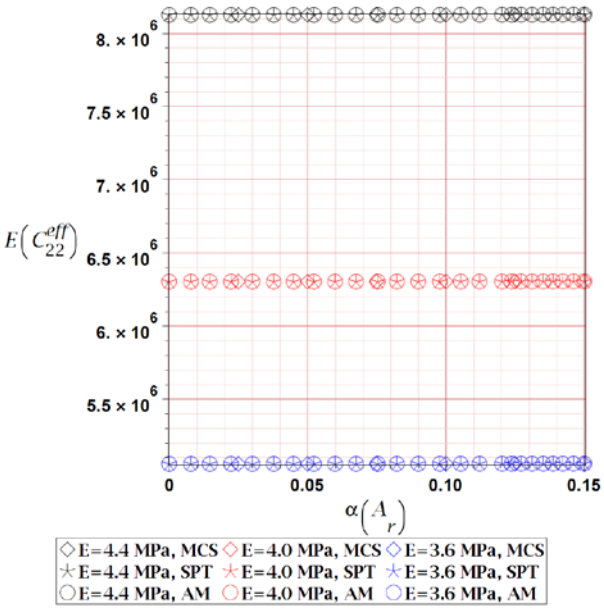

Figure 3. Expected value $E\left(C_{22}^{eff}\right)$ for an increasing matrix Young modulus E_m w.r.t. coefficient of variation of particle aspect ratio $\alpha(A_r)$.

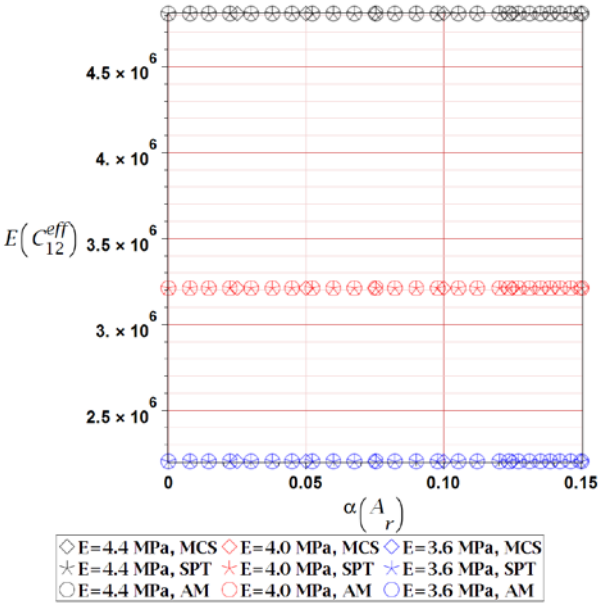

Figure 4. Expected value $E\left(C_{12}^{eff}\right)$ for an increasing matrix Young modulus E_m w.r.t. coefficient of variation of particle aspect ratio $\alpha(A_r)$.

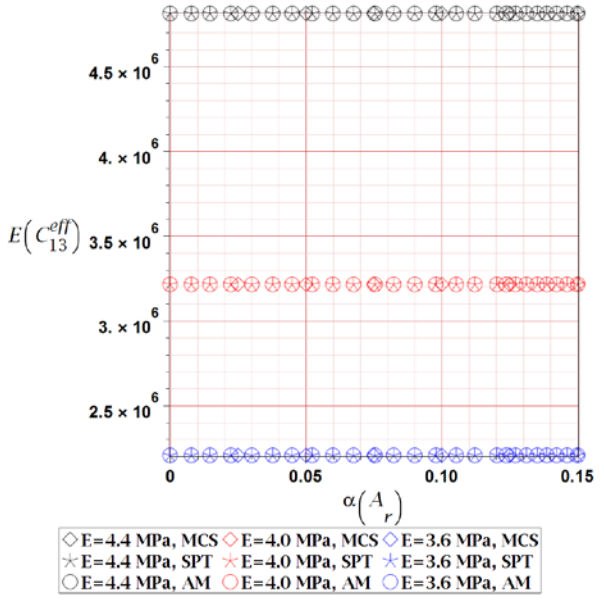

Figure 5. Expected value $E\left(C_{13}^{eff}\right)$ for an increasing matrix Young modulus E_m w.r.t. coefficient of variation of particle aspect ratio $\alpha(A_r)$.

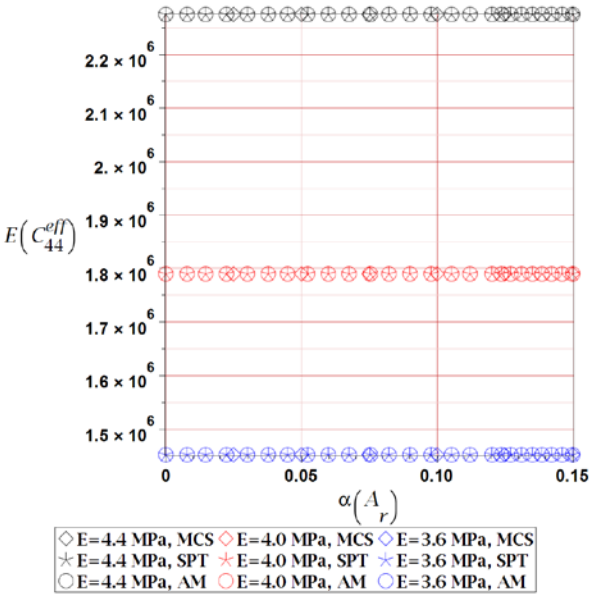

Figure 6. Expected value $E\left(C_{11}^{eff}\right)$ for an increasing matrix Young modulus E w.r.t. coefficient of variation of particle aspect ratio $\alpha(A_r)$.

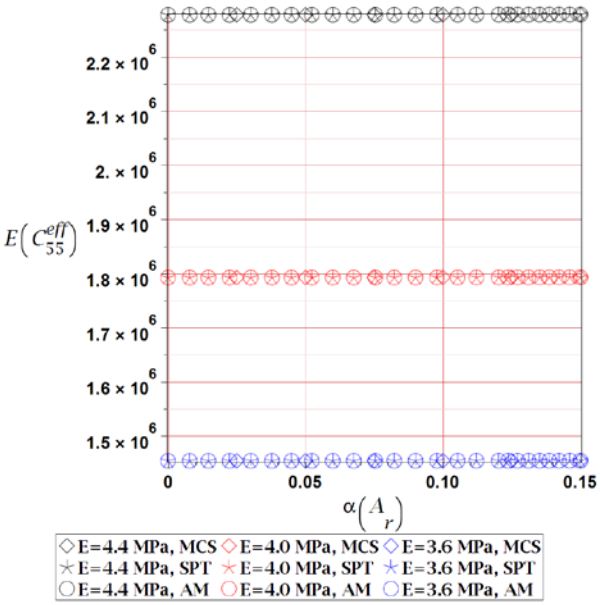

Figure 7. Expected value $E\left(C_{11}^{eff}\right)$ for an increasing matrix Young modulus E w.r.t. coefficient of variation of particle aspect ratio $\alpha(A_r)$.

Coefficients of variation $\alpha\left(C_{ij}^{eff}\right)$ are depicted on Figure 8 till Figure 13 and are at least 20 times smaller than the input ones. This means that homogenization considerably decreases the uncertainty. They almost linearly increase together with $\alpha(A_r)$, perfectly agree for all the three probabilistic methods and decrease together with an increase of mechanical properties of the matrix. Unlike the $E\left(C_{ij}^{eff}\right)$, $\alpha\left(C_{ij}^{eff}\right)$ differ significantly for the groups of components up to 60 times, which is reported for $\alpha\left(C_{44}^{eff}\right)$ vs. $\alpha\left(C_{55}^{eff}\right)$. The highest coefficient of variation is reported for C_{13}^{eff} and the lowest – for C_{12}^{eff}.

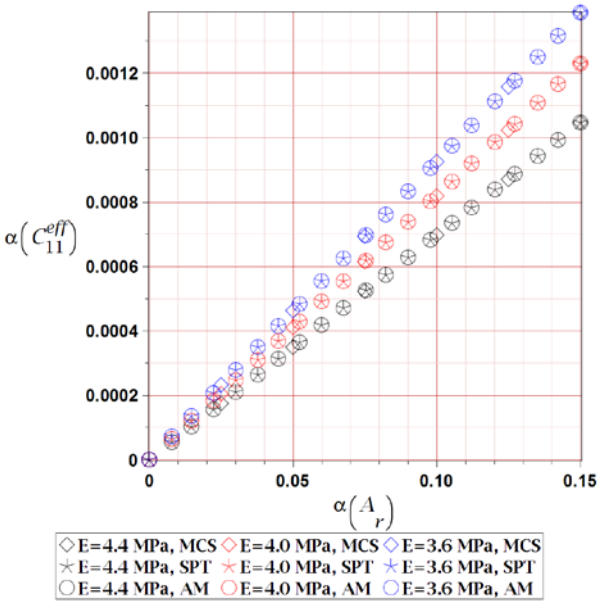

Figure 8. Coefficient of variation $\alpha\left(C_{11}^{eff}\right)$ for an increasing matrix Young modulus E_m w.r.t. coefficient of variation of particle aspect ratio $\alpha(A_r)$.

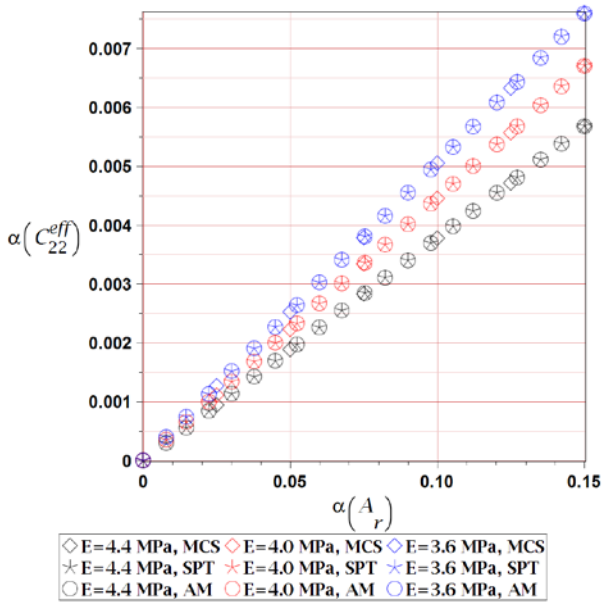

Figure 9. Coefficient of variation $\alpha\left(C_{22}^{eff}\right)$ for an increasing matrix Young modulus E_m w.r.t. coefficient of variation of particle aspect ratio $\alpha(A_r)$.

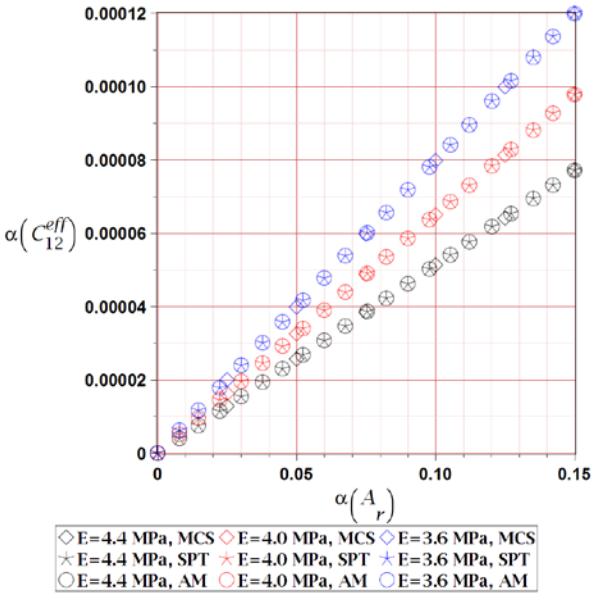

Figure 10. Coefficient of variation $\alpha\left(C_{12}^{eff}\right)$ for an increasing matrix Young modulus E_m w.r.t. coefficient of variation of particle aspect ratio $\alpha(A_r)$.

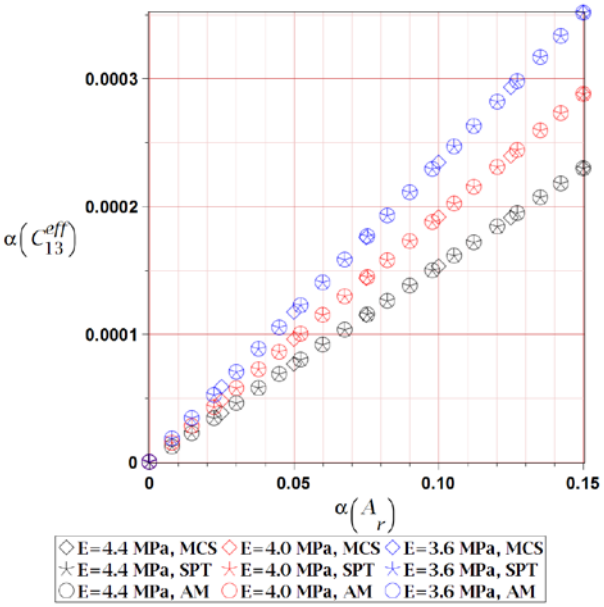

Figure 11. Coefficient of variation $\alpha\left(C_{13}^{eff}\right)$ for an increasing matrix Young modulus E_m w.r.t. coefficient of variation of particle aspect ratio $\alpha(A_r)$.

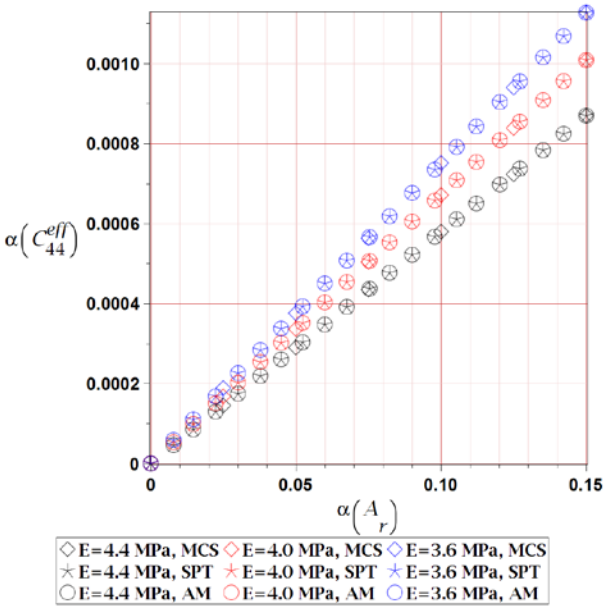

Figure 12. Coefficient of variation $\alpha\left(C_{44}^{eff}\right)$ for an increasing matrix Young modulus E_m w.r.t. coefficient of variation of particle aspect ratio $\alpha(A_r)$.

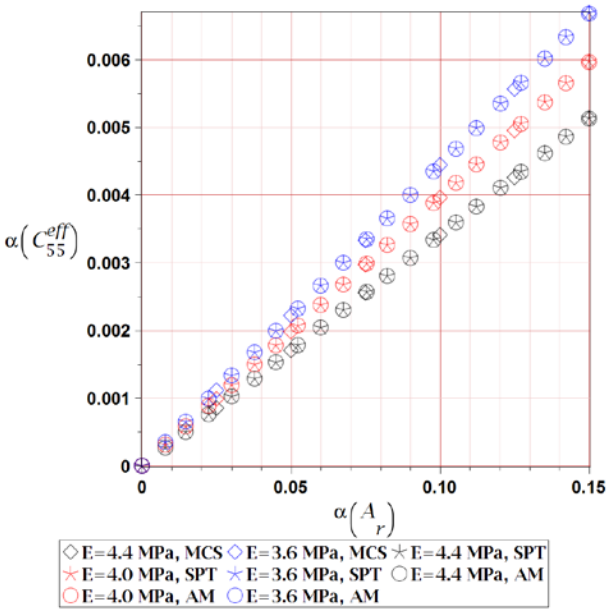

Figure 13. Coefficient of variation $\alpha\left(C_{55}^{eff}\right)$ for an increasing matrix Young modulus E_m w.r.t. coefficient of variation of particle aspect ratio $\alpha(A_r)$.

Skewness of the homogenized stiffness tensor $\beta\left(C_{ij}^{eff}\right)$ are presented on Figure 14 till Figure 19. It starts from 0 for a null uncertainty, almost linearly increases with an increase of $\alpha(A_r)$ and reach maximum magnitude between 0.02 and 0.3 for $\alpha(A_r) = 0$. All skewnesses are positive and in majority of them, a small concavity is visible. They differ for particular components by an order of magnitude so that in each stretch group one skewnesses is at least 10 times higher than the other (see Figure 14 and Figure 15). The SPT and AM return here perfectly the same result, while the MCS shows quite a significant scatter for all stiffness tensor components having small magnitude, i.e. C_{11}^{eff}, C_{13}^{eff} and C_{44}^{eff}. Quite importantly, a change in mechanical properties of the matrix does not have an impact on the skewness – the differences are marginal and much below a single percent.

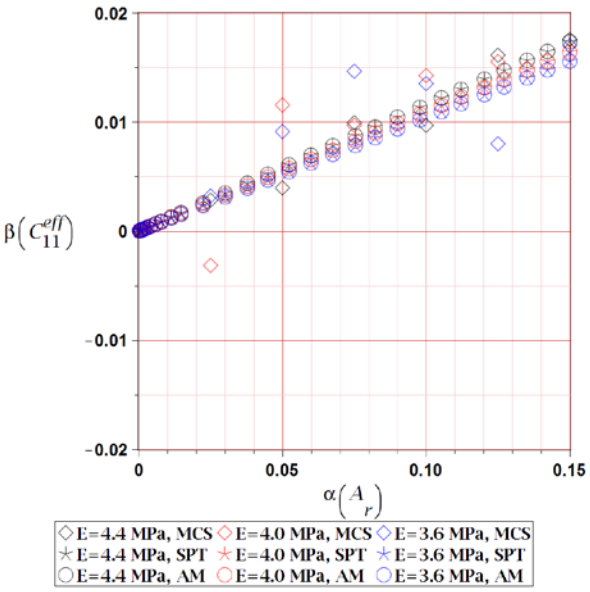

Figure 14. Skewness $\beta\left(C_{11}^{eff}\right)$ for an increasing matrix Young modulus E_m w.r.t. coefficient of variation of particle aspect ratio $\alpha(A_r)$.

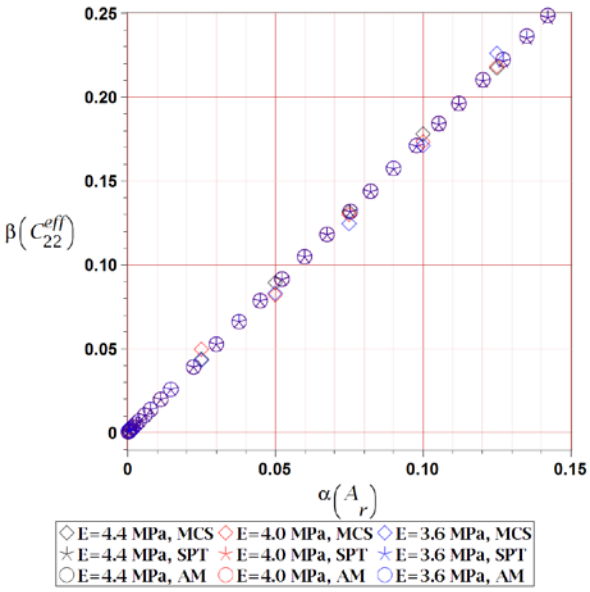

Figure 15. Skewness $\beta\left(C_{22}^{eff}\right)$ for an increasing matrix Young modulus E_m w.r.t. coefficient of variation of particle aspect ratio $\alpha(A_r)$.

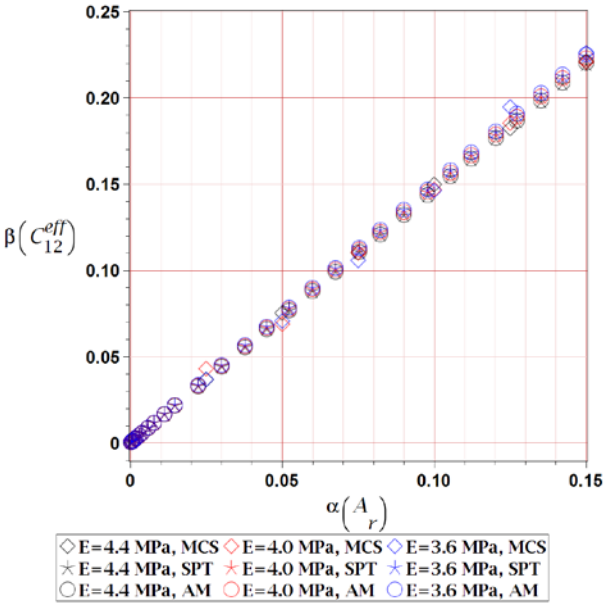

Figure 16. Skewness $\beta\left(C_{12}^{eff}\right)$ for an increasing matrix Young modulus E_m w.r.t. coefficient of variation of particle aspect ratio $\alpha(A_r)$.

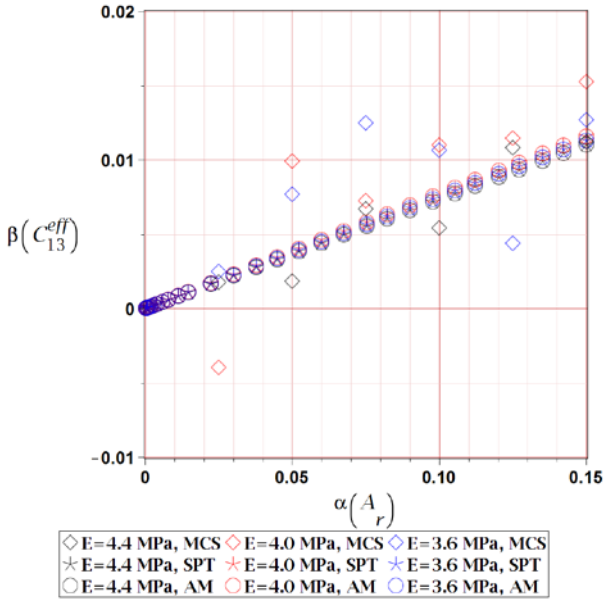

Figure 17. Skewness $\beta\left(C_{13}^{eff}\right)$ for an increasing matrix Young modulus E_m w.r.t. coefficient of variation of particle aspect ratio $\alpha(A_r)$.

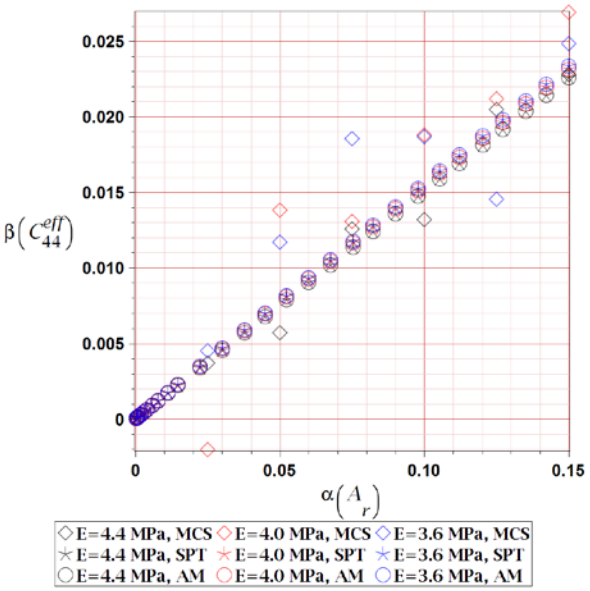

Figure 18. Skewness $\beta\left(C_{44}^{eff}\right)$ for an increasing matrix Young modulus E_m w.r.t. coefficient of variation of particle aspect ratio $\alpha(A_r)$.

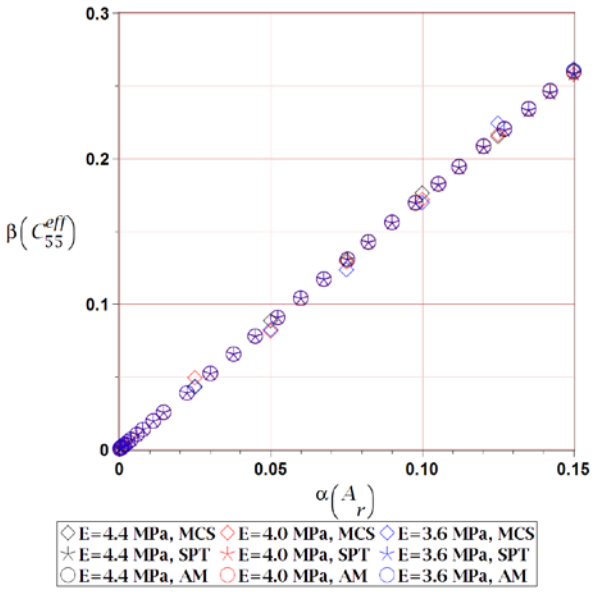

Figure 19. Skewness $\beta\left(C_{55}^{eff}\right)$ for an increasing matrix Young modulus E_m w.r.t. coefficient of variation of particle aspect ratio $\alpha(A_r)$.

Graphs of kurtosis $\kappa\left(C_{ij}^{eff}\right)$ are assembled in Figure 20 till Figure 25 and presented in relation to $\alpha(A_r)$. They are all positive and increasing with an increase of the input uncertainty in a convex manner. The only exception for this rule is $\kappa\left(C_{13}^{eff}\right)$, where the AM returns a small convexity. Similarly to the skewness, kurtoses of coefficients from the same groups of stretches differ in magnitude several times and the MCS shows a large scatter for coefficients having small kurtoses. The three probabilistic methods lose perfect convergence for kurtosis and, by this, it is not uniquely defined with $\alpha(A_r)$. The SPT serves for the lower limit of approximation, the MCS – for the higher limit (when no MCS scatter occurs) and the AM usually stays in the middle. This discrepancy increases together with an increase of $\alpha(A_r)$ and reaches maximally 75% for C_{22}^{eff}. Difference is generally smaller between AM and SPT especially for kurtoses with small magnitude, i.e. $\kappa\left(C_{11}^{eff}\right)$, $\kappa\left(C_{13}^{eff}\right)$ and $\kappa\left(C_{44}^{eff}\right)$ and for $\kappa\left(C_{11}^{eff}\right)$ it does not exist. Tuning of mechanical properties of the matrix does not have an influence on kurtosis of the stiffness tensor. Differences are only visible for the MCS, but this method proves to be unreliable for determination of $\kappa\left(C_{ij}^{eff}\right)$ because of a large scatter reported for half of coefficients.

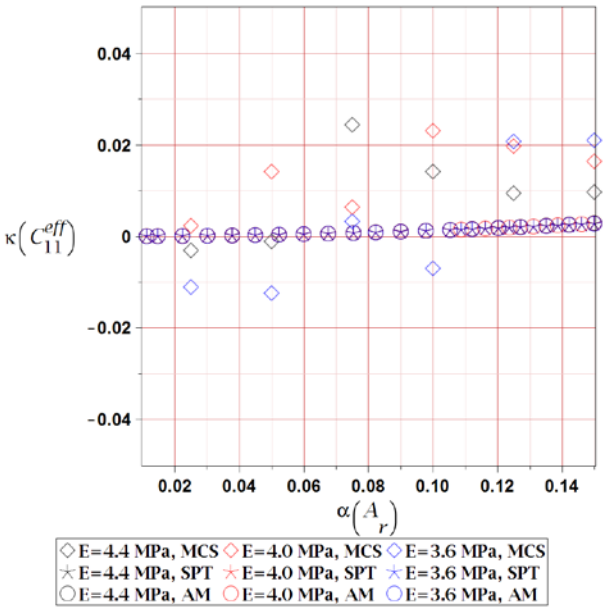

Figure 20. Kurtosis $\kappa\left(C_{11}^{eff}\right)$ for an increasing matrix Young modulus E_m w.r.t. coefficient of variation of particle aspect ratio $\alpha(A_r)$.

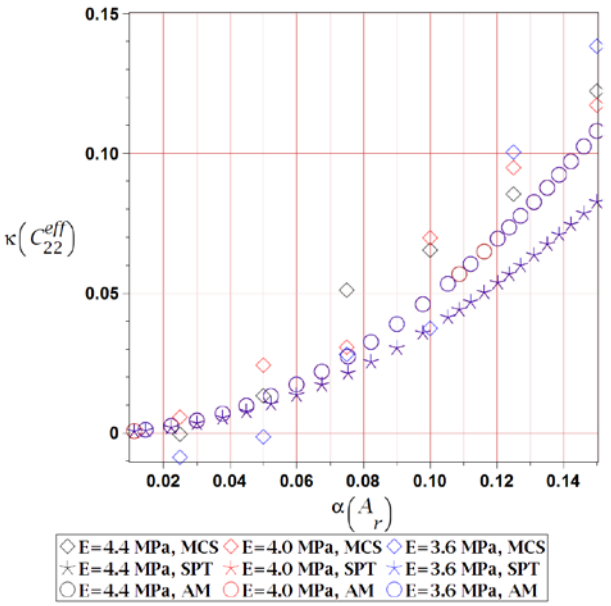

Figure 21. Kurtosis $\kappa\left(C_{22}^{eff}\right)$ for an increasing matrix Young modulus E_m w.r.t. coefficient of variation of particle aspect ratio $\alpha(A_r)$.

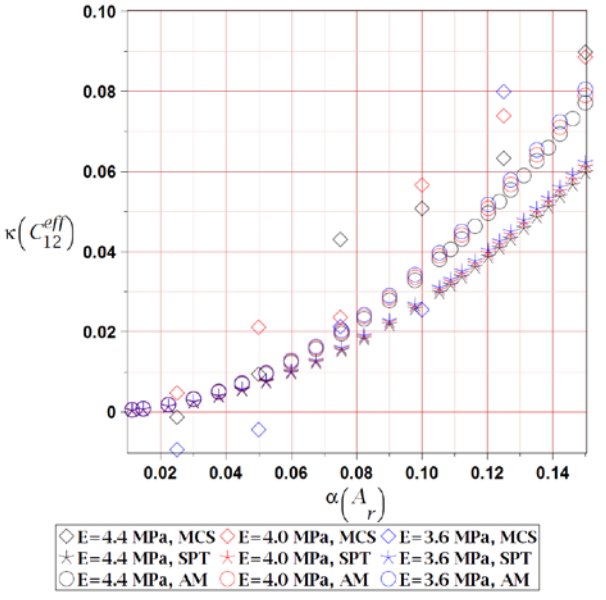

Figure 22. Kurtosis $\kappa\left(C_{12}^{eff}\right)$ for an increasing matrix Young modulus E_m w.r.t. coefficient of variation of particle aspect ratio $\alpha(A_r)$.

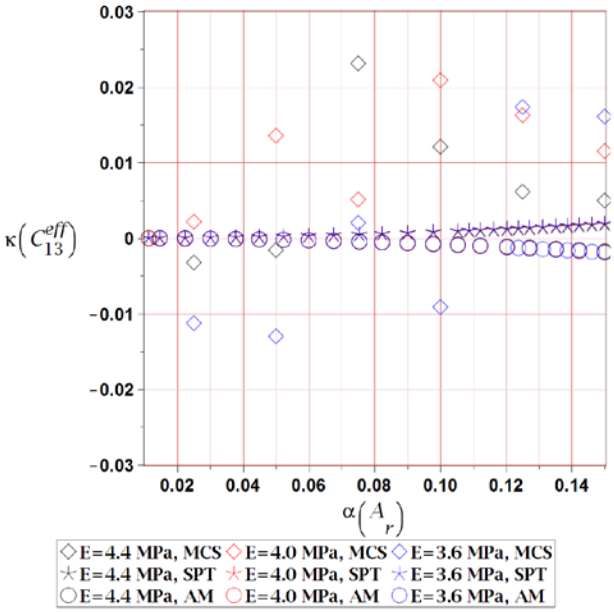

Figure 23. Kurtosis $\kappa\left(C_{13}^{eff}\right)$ for an increasing matrix Young modulus E_m w.r.t. coefficient of variation of particle aspect ratio $\alpha(A_r)$.

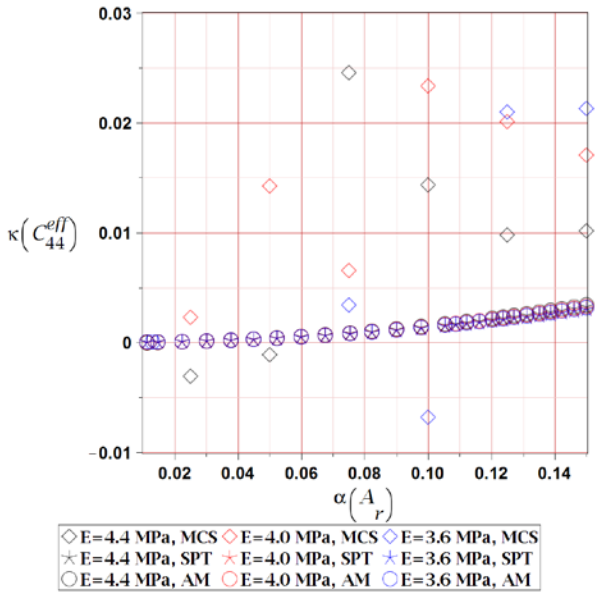

Figure 24. Kurtosis $\kappa\left(C_{44}^{eff}\right)$ for an increasing matrix Young modulus E_m w.r.t. coefficient of variation of particle aspect ratio $\alpha(A_r)$.

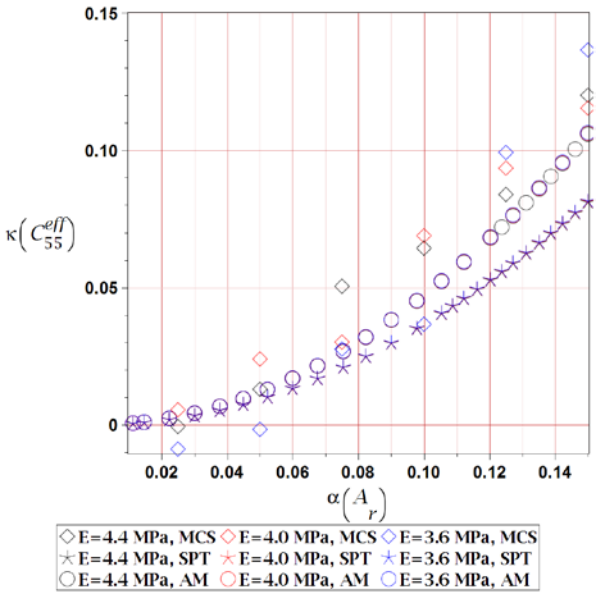

Figure 25. Kurtosis $\kappa\left(C_{55}^{eff}\right)$ for an increasing matrix Young modulus E_m w.r.t. coefficient of variation of particle aspect ratio $\alpha(A_r)$.

Conclusions

This work presents a successful study of probabilistic characteristics of the homogenized random orthotropic effective stiffness tensor C_{ij}^{eff} coming from a single-particle RVE. Randomness in this study comes from an uncertain aspect ratio A_r of ellipsoidal reinforcing particle and it is based on a high range of $A_r \in \left[\frac{1}{7}, \frac{50}{1}\right]$. This is done for increasing mechanical characteristics of the matrix, i.e. Young modulus E_m and Poisson ratio ν_m in the ranges of $E_m \in \{3.6, 4.0, 4.4\}\, MPa$ and $\nu_m \in \{0.374, 0.34, 0.306\}$. Middle values of these characteristics aim to represent properties of the HDPU in its linear regime. Methodology applied for retrieval of these random characteristics is triple. Firstly, a framework of the Iterative Stochastic Finite Element Method is applied, secondly a crude Monte Carlo simulation is utilized and finally the semi-analytical method is used. All these methods are based on polynomial approximations of the discrete results of stiffness tensor components coming from homogenization of RVE modelled and computed in the FEM.

This study proves that for a Gaussian aspect ratio the resulting stiffness tensor C_{ij}^{eff} is not exactly Gaussian and has a non-zero skewness and kurtosis. It also shows that the homogenization dampens the initial uncertainty so that the resulting stiffness tensor has lower variation than the input one and that the increase in initial uncertainty only marginally decreases the expected values of stiffness tensor. An increase of mechanical properties of the matrix has a visible effect only on the coefficients of variation of the homogenized stiffness tensor $\alpha\left(C_{ij}^{eff}\right)$. Other probabilistic characteristics are not affected by this variable, at least within the considered limits. The coefficient of variation, skewness and kurtosis of C_{ij}^{eff} all have a major difference in magnitude for the corresponding stretches coming from the same type of boundary conditions, i.e. for uniaxial and biaxial tension as well as uniaxial shear. This is because of the different course of relation of these coefficients relative to the particle aspect ratio A_r. The randomness for uniaxial tension coefficients is higher in the axis where

prolate particle had its main axis and biaxial tension as well as uniaxial shear is much more random for axes where oblate particle had its main axes. It is worth to mention that $\alpha(C_{ij}^{eff})$, $\beta(C_{ij}^{eff})$ and $\kappa(C_{ij}^{eff})$ are all increasing with an increase of an input uncertainty so that the homogenized stiffness tensor is less Gaussian with an increase of this input uncertainty. Agreement of the three probabilistic methods is perfect for $E(C_{ij}^{eff})$ and $\alpha(C_{ij}^{eff})$ and the Monte-Carlo simulation diverges from other methods for $\beta(C_{ij}^{eff})$ and $\kappa(C_{ij}^{eff})$. This is especially visible for stiffness tensor coefficients which have a small magnitude of probabilistic characteristics, where this method has a major scatter. The ISFEM and semi-analytical approach lose convergence solely for $\kappa(C_{ij}^{eff})$, but for majority of C_{ij}^{eff} they still return a similar result, which is always smooth and without any local effects.
Further ISFEM computational studies will concern numerical simulation of the RVE with matrix and an interphase in its hyper-elastic regime for particulate composites with spherical reinforcement. An additional interesting extension of this work would be inclusion of the random interphase in-between the two current composite constituents and verification of its influence on the behavior of this composite.

References

[1] Dinzart, F. and Sabar, H. (2017) New micromechanical modeling of the elastic behavior of composite materials with ellipsoidal reinforcements and imperfect interfaces, *International Journal of Solids and Structures* **108**, 254–262.

[2] Zhang, Y., Dai, K., Tang, J., Ji, X. and Li, Z. (2010) Anisotropically conductive polymer composites with a selective distribution of carbon black in an in situ microfibrillar reinforced blend, *Materials Letters* **64**, 1430-1432.

[3] Levin, V. and Markov, M. (2016) Effective thermal conductivity of micro-inhomogeneous media containing imperfectly bonded ellipsoidal inclusions, *International Journal of Engineering Science* **109**, 202–215.

[4] Lavergne, F., Sab, K., Sanahuja, J., Bornert, M., Toulemonde, C. (2016) An approximate multiscale model for aging viscoelastic materials exhibiting time-dependent Poisson's ratio, *Cement and Concrete Research* **86**, 42-54.

[5] Avazmohammadi, R. and Castañeda, P. (2013) Tangent Second-Order Estimates for the Large-Strain, Macroscopic Response of Particle-Reinforced Elastomers, *Journal of Elasticity* **112**, 139–183.

[6] Kamiński, M. and Sokołowski, D. (2016) Dual probabilistic homogenization of the rubber-based composite with random carbon black particle reinforcement, *Composite Structures* **140**, 783–797.

[7] Sokołowski, D. and Kamiński, M. (2018) Computational homogenization of carbon/polymer composites with stochastic interface defects, *Composite Structures* **183**, 434-449.

[8] Saavas, D., Stefanou, G., Papadrakakis, M. (2016) Determination of RVE size for random composites with local volume fraction variation, *Computer Methods in Applied Mechanics and* Engineering **305**, 340-358.

[9] Sohn, D. (2018) Periodic mesh generation and homogenization of inclusion-reinforced composites using an element-carving technique with local mesh refinement, *Composite Structures* **185**, 65-80.

[10] Parnell, W. J., (2016) The Eshelby, Hill, Moment and Concentration Tensors for Ellipsoidal Inhomogeneities in the Newtonian Potential Problem and Linear Elastostatics, *Journal of Elasticity* **125**, 231–294.

[11] Sabina, F. J., Gandarrilla-Pérez, C. A., Otero, J. A., Rodríguez-Ramos, R., Bravo-Castillero, J., Guinovart-Díaz R. and Valdiviezo-Mijangos, O. (2015) Dynamic homogenization for composites with embedded multioriented ellipsoidal inclusions, *International Journal of Solids and Structures* **69**–**70**, 121–130.

[12] Parsaee, A., Shokrieh, M. M. and Mondali, M. (2016) A micro–macro homogenization scheme for elastic composites containing high volume fraction multi-shape inclusions, *Computational Materials Science* **121**, 217–224.

[13] Kamiński, M. (2013) The Stochastic Perturbation Technique for Computational Mechanics, Wiley, Chichester.

[14] Kamiński, M. (2015) On the dual iterative stochastic perturbation-based finite element method in solid mechanics with Gaussian uncertainties, *International Journal for Numerical Methods in Engineering* **104**, 1038-1060.